Nat Hazards (2013) 65:477–495
DOI 10.1007/s11069-012-0378-z

ORIGINAL PAPER

A fast GIS-based risk assessment for tephra fallout: the example of Cotopaxi volcano, Ecuador

Part I: probabilistic hazard assessment

Sebastien Biass · Costanza Bonadonna

Received: 15 February 2012 / Accepted: 30 August 2012 / Published online: 16 September 2012

Abstract We present a comprehensive probabilistic hazard assessment for tephra fallout of Cotopaxi volcano (Ecuador), a quiescent but active stratovolcano known for its highly explosive behaviour. First, we developed a set of possible eruptive scenarios based on thorough field investigations, literature studies and using the Global Volcanism Program (GVP) database. Five eruption scenarios were identified, including two based on large pre-historical sub-Plinian/Plinian eruptions with eruptive parameters constrained from field investigations (One Eruption Scenario; OES) and three Eruption Range Scenarios (ERS) based on the Volcanic Explosivity Index (VEI) classification, for which eruptive parameters (i.e. erupted volume, plume height and median grainsize) were stochastically sampled within boundaries defined by VEI 3, 4 and 5. Second, the modelling was performed using the advection-diffusion model TEPHRA2 in combination with wind profiles from the NOAA NCEP/NCAR Reanalysis 1 database. We performed 1,000 runs for each eruption scenario, stochastically sampling a wind profile (OES and ERS) and a set of eruptive parameters (ERS only) at each run. Using the conditional probabilities of occurrence of eruption of VEI 3, 4 and 5 calculated from the GVP catalogue, we assessed the probability of tephra accumulation in a given time window. Based on the GVP database, a simple Poisson model shows that an eruption of VEI $\geq$3 has a 36 % probability of occurrence in the next 10 years. Finally, the hazard assessment was compiled based on three different outputs, including (i) probability maps for a given tephra accumulation, (ii) isomass maps for a given probability value and (iii) hazard curves for a given location. We conclude that the area west of Cotopaxi is exposed to light to severe tephra fallout for the smallest eruption magnitude considered (i.e. VEI 3). This area comprises a main communication axis (Panamerican Highway) topographically constrained at the bottom of the Interandean

Electronic supplementary material The online version of this article (doi:10.1007/s11069-012-0378-z) contains supplementary material, which is available to authorized users.

S. Biass (✉) · C. Bonadonna
Section of Earth and Environmental Sciences, University of Geneva, 13, rue des Maraichers, 1205 Geneva, Switzerland
e-mail: sebastien.biasse@unige.ch

Valley, as well as the capital Quito and the town of Latacunga. In a companion paper, Biass et al. (this volume) propose a method for a rapid risk assessment for tephra fallout using global and easily accessible data and the hazard assessment described here.

Keywords Volcanic hazard · Tephra · Probabilistic hazard assessment · Cotopaxi · Ecuador

1 Introduction

Providing authorities with comprehensive eruption scenarios for sustainable land-use planning and efficient tools for decision-making is a key objective of modern volcanology. The complexity of hazard assessments comes from the fact that: (i) volcanic activity is usually the result of interactions between many independent physical and geological processes acting over different time scales (Mendoza-Rosas and la Cruz-Reyna 2008); (ii) the effects of large eruptions are less assimilated by the public compared with other natural phenomenon such as earthquakes, tsunamis or hurricanes, due to their rare occurrence; (iii) explosive eruptions typically produce a wide range of hazardous phenomena that require independent studies; and (iv) the constant population increase results in more exposed critical infrastructure on which modern societies depend (Blong 1984; Simkin and Siebert 1994; Johnston et al. 2000; Small and Naumann 2001; Moteff et al. 2003; Hellström 2007).

It is nowadays broadly accepted that the fulfilment of a comprehensive risk assessment includes three necessary steps (Fournier d'Albe 1979; Mendoza-Rosas and la Cruz-Reyna 2008). First, the assessment of the hazard aims at evaluating the nature, the return period and the extent of hazardous phenomena. Second, the vulnerability assessment evaluates the likelihood of the exposed elements to be affected by a given threat. Finally, the risk assessment is a convolution of the two previous aspects.

Thorough risk assessments typically require a large number of data and information difficult to obtain (e.g. field data, wind profiles, recurrence of tephra production, geographical information, location of critical facilities). This paper presents a probabilistic hazard assessment for tephra fallout associated with moderate to large explosive eruptions of Cotopaxi volcano (Ecuador), based on global and easily accessible databases (Fig. 1). Tephra, referring here to all particles produced during an explosive volcanic eruption regardless of size or composition, is usually not a direct cause of fatalities (Blong 1984; Siebert and Simkin 2002). Nevertheless, due to the large area it typically affects ($\geq$10 km for moderate eruptions of VEI 3), it can impact several aspects of modern societies resulting in complex risk patterns (Hill et al. 1998; Connor et al. 2001). Table 1 provides examples of exposed elements likely to be impacted by the fallout of tephra. A probability assessment of eruptions of each VEI class was performed based on the data from the Global Volcanism Program of the Smithsonian Institution (Siebert and Simkin 2002) and a statistical analysis of wind patterns achieved using the NOAA NCEP/NCAR Reanalysis 1 database (Kalnay et al. 1996). A companion paper (Biass et al., this volume) proposes a risk assessment around Cotopaxi, which combines the outcome of the present paper with a thematic vulnerability assessment using free and easily accessible geo-referenced data. The whole analysis was performed using GIS softwares, allowing for new ways of combining hazard and vulnerability assessments into a qualitative risk assessment.

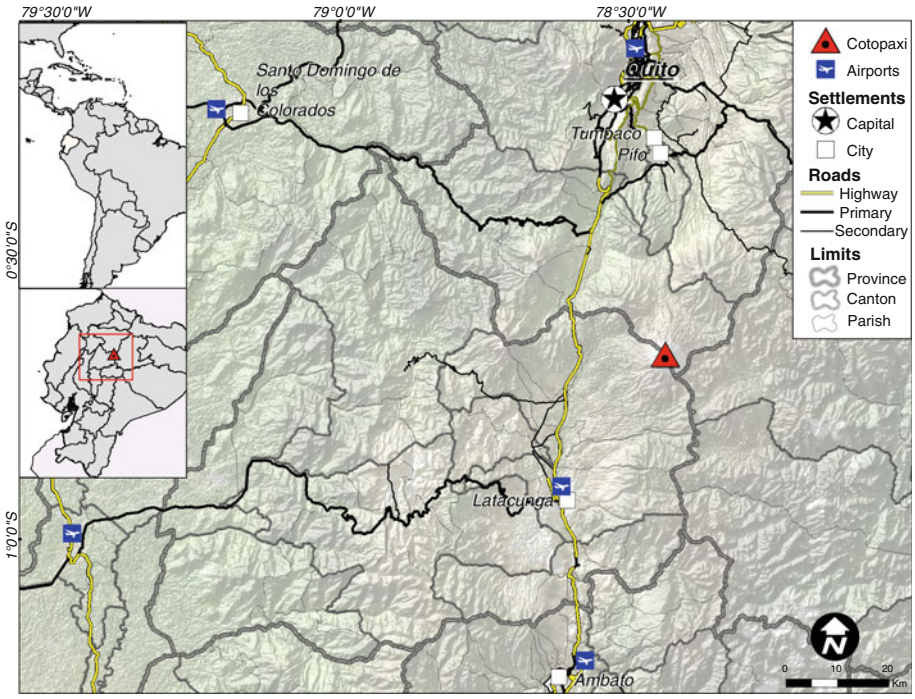

Fig. 1 Overview map around Cotopaxi volcano, showing three levels of administrative units (provinces, cantons and parishes), the main cities, airports, the road network and the topographic context. Quito and Latacunga are located 50 km north and 35 km south of Cotopaxi volcano, respectively

Table 1 A non-exhaustive list of references treating various impacts of tephra fallout

Exposed element	References
Health	Horwell et al (2003), Horwell and Baxter (2006), Wilson et al (2011b)
Buildings	Blong (1984, 2003), Spence et al (1996, 2005), Pomonis et al (1999)
	Marti et al (2008), Zuccaro et al (2008)
Lifelines	Chester et al (2000), Johnston et al (2000), Wilson et al (2011a)
Economy	Johnston et al (2000), Wilson et al (2012)
Environment	Inbar et al (1995), Robock (2000), Millard et al (2006)
	Martin et al (2009)

2 Geological background

Ecuador (256,000 km^2) is geographically divided in three distinct zones: *La Costa* (west), *La Sierra* (highlands, centre) and *La Amazonia* (east), of which the first two comprise most of Ecuador's 13 million inhabitants (Fig. 1). Historical reports of volcanic activity at Cotopaxi begin during Spanish conquests in 1534. According to the EM-DAT database (EM-DAT 2011), volcanic eruptions are the second most important natural hazard in Ecuador in terms of number of affected people, with floods affecting even more.

Cotopaxi (0.68°S 78.44°W, 5,897 m a.s.l., Fig. 1) is located in the Eastern Cordillera of the Ecuadorian Andes in the Northern Volcanic Zone, with a cone that rises 2,900 m above the highlands of the Interandean Depression (Mothes et al. 2004; Aguilera et al. 2004). This edifice of a diameter of 20 km dominates two populated provinces: the province of Pichincha in the north, which includes Ecuador's capital Quito, and the province of Cotopaxi in the south, with its capital Latacunga. The Panamerican Highway, a trunk road running N-S, goes by the western side of the volcanic edifice in the Interandean Valley. In addition, the main rail-road connecting the capital Quito to Ecuador's largest city Guayaquil is located at the bottom of the Interandean Valley.

For at least the past 4,000 years, the eruptive activity of Cotopaxi volcano has been mainly dominated by andesitic magmatism (Hall and Mothes 2008; Pistolesi et al. 2011), including 22 layers of tephra fallout described by Barberi et al. (1995) for the past 2,000 years. Historical activity at Cotopaxi has been characterized by the effusion of lava flows and moderate to strong explosive episodes, which have always triggered lahars through partial melting of the ice cap (Barberi et al. 1992, 1995). The town of Latacunga has been heavily affected by lahars following the eruptions of 1742, 1768 and 1877 (Mothes et al. 2004; Aguilera et al. 2004).

Most of the recent literature available on Cotopaxi describes tephra deposits and their ability to generate lahars (e.g. Barberi et al. 1992, 1995; Mothes et al. 2004; Aguilera et al. 2004; Pistolesi et al. 2011), with some examples of multi-hazard risk assessments (D'Ercole 1996; D'Ercole and Demoraes 2003). However, comprehensive hazard assessments of tephra fall are still missing for most of Ecuadorian volcanoes, even though the country is often affected by tephra fall episodes. For example, the November 3, 2002 eruption of the nearby Reventador volcano produced a blanket of tephra of 3–5 mm over the Mariscal Sucre International Airport in Quito, closing the airport for 8 days as a result of ash deposition on runways and airplanes (Guffanti et al. 2009). In addition, tephra resulting from the August 16, 2006 eruption of Tungurahua affected more than 300,000 people and was responsible for losses in agriculture of about $150 million (EM-DAT 2011).

Accurate tephrostratigraphic investigations are a necessary step towards the development of comprehensive explosive eruption scenarios, but do not constitute comprehensive hazard and risk assessments. In order to help the development of effective mitigation measures, both the recurrence rate of tephra production and its dispersal need to be assessed, in combination with the identification of the various geographical areas that will be affected.

3 Method

Hazard assessments for tephra accumulation typically require the development of eruption scenarios determined from the study of the eruptive history of a volcano. Such parameters include plume height, erupted mass, eruption duration and grainsize distribution. Hazard assessments also require wind data and a calculation grid. Each of these items is discussed below.

3.1 Eruptive history

The reconstruction of the eruptive history of a given volcano is typically achieved through thorough field investigations. Two of the largest eruptions of Cotopaxi (i.e. Layer 3 and

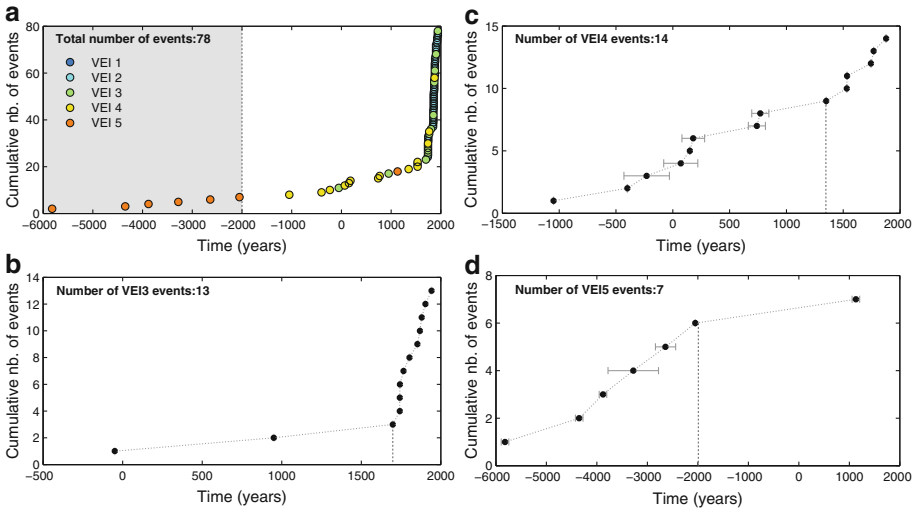

Fig. 2 Eruptive trend inferred from the GVP database; **a** complete record showing the rhyolitic period (*grey*) and the andesitic period (*white*); **b** VEI = 3; **c** VEI = 4 and **d** VEI = 5. *Vertical dashed lines* show the break in slope used to define the complete record

Layer 5) have been characterized by Biass and Bonadonna (2011). When no detailed field data are available, one alternative solution is to use eruption databases, such as the Global Volcanism Program (GVP; Siebert and Simkin 2002). For example, Fig. 2a shows the cumulative number of eruptions of any VEI at Cotopaxi volcano, based on the GVP database. This study focuses on VEIs 3 to 5, as a VEI 3 is the minimum size of eruption considered to be a threat to populations in this area and VEI 5 is the largest category of events in the history of Cotopaxi volcano. Figure 2b–d shows the cumulative number of eruptions of VEI 3, 4 and 5, respectively.

3.2 Wind data

The hazard assessment presented here uses wind profiles from the NOAA NCEP/NCAR Reanalysis 1 database (Kalnay et al. 1996), which provides 4-daily measurements of wind velocity and direction for 17 pressure levels, from 1948 to present on a 2.5° × 2.5° degrees grid. Figure 3a, b shows wind velocities and directions for the 1997–2008 period for the median of the whole dataset (±standard deviation) and the median of each separate year, respectively. Figure 4 shows the probability of the wind blowing in a given direction and the wind velocity (bins are 20°) at each altitude and for the whole dataset. Figures 3 and 4 show dominant westward wind directions between ground level and about 15 km, in agreement with the dispersal axis inferred from isomass maps for previous eruptions (Biass and Bonadonna 2011). Figure 4 shows a >50 % probability of wind blowing in a west sector for the same altitudes, and a ∼90 % probability of wind blowing in a sector comprised between 240° and 300° between vent level and about 13 km. In order to investigate the influence of El Niño/La Niña phenomena on the distribution of wind profiles, we have considered two important events (1982–1983 and 1997–1998) without finding any particular trend (Fig. 3c, d).

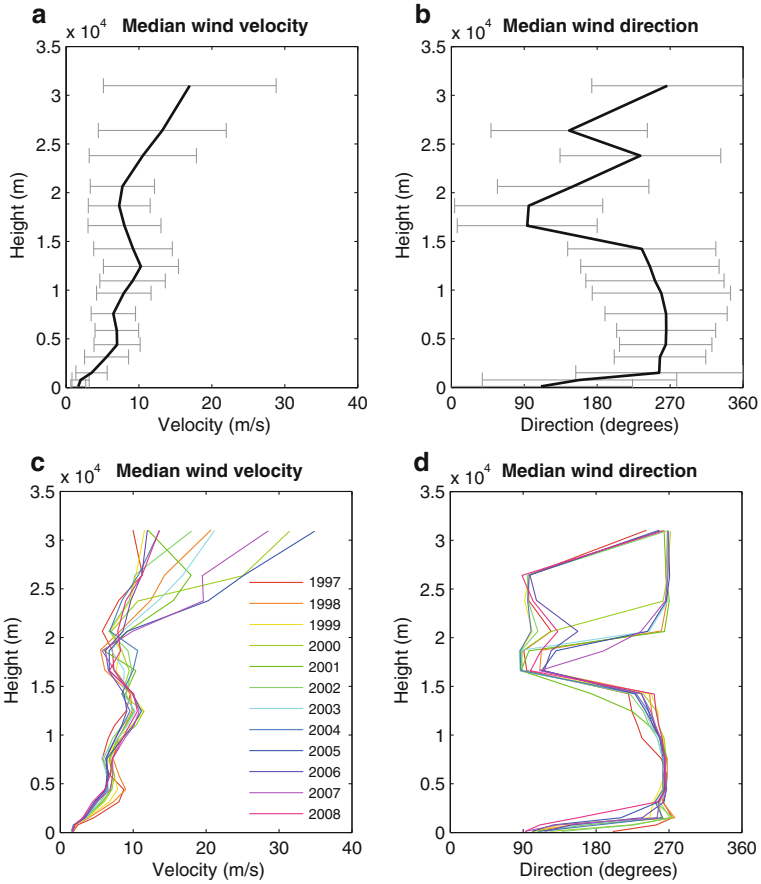

Fig. 3 Wind profiles showing the **a** median velocity and **b** median direction the wind blows to for the years 1997–2008. *Error bars* indicate the standard deviation. The median of each year is also shown for **c** wind velocity and **d** wind direction

3.3 Calculation grid

Tephra dispersal models usually require a geo-referenced grid for calculation purposes. One convenient way of obtaining these grids is to use free and global digital elevation models (DEM), such as the NOAA Global Land 1-km Base Elevation Project (GLOBE) or the CGIAR-CSI SRTM 90 m. We used here a modified version of the GLOBE DEM, setting the resolution of the model output to 1 km, which provides a good compromise between accuracy at a large scale and computing time. The size of the calculation grid in this study is 350 × 250 km, that is, 88,294 calculation nodes.

4 Hazard assessment

Numerical simulations are valuable tools that can help to infer parts of deposits that are either inaccessible or removed by erosion, but require inputs that are usually empirically

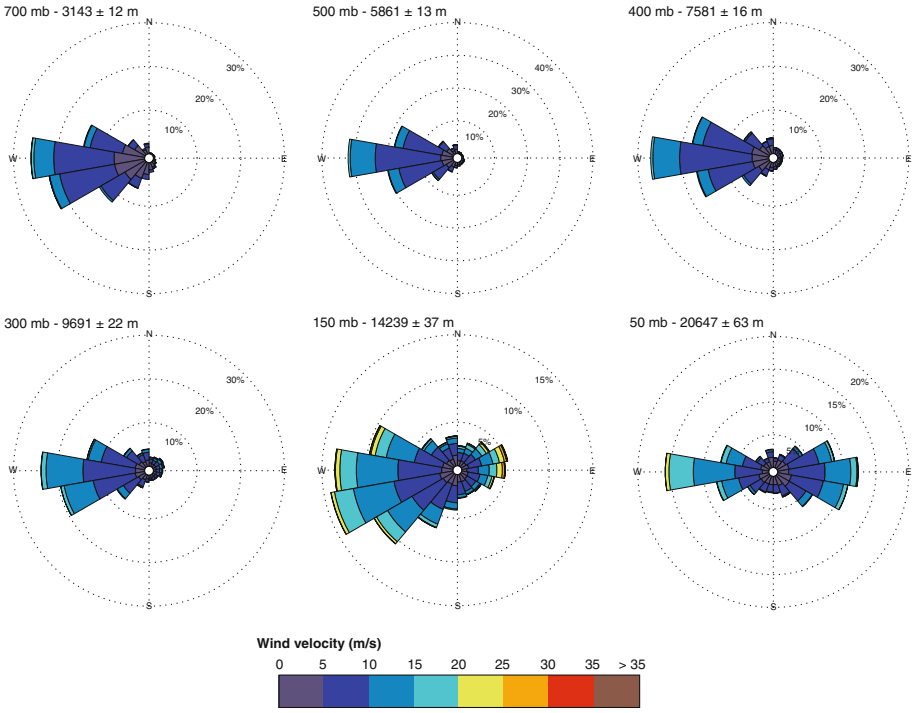

Fig. 4 Probability of wind blowing to a given direction (bins = 20°) at selected altitudes and for all years

chosen with the assumption that future activity will be similar to past activity, or will follow the current trend. In addition, a probabilistic approach helps to describe the uncertainty associated with complex volcanic processes, which is required for mitigation measures of potentially affected communities.

We use event trees similar to those proposed by Newhall and Hoblitt (2002) and Neri et al (2008) in simplified forms, considering two different time windows (Fig. 5). First, we assessed the probability of tephra accumulation at given coordinates for an eruption of a given intensity as basic information for emergency management (i.e. evaluation of node 3, knowing an eruption of a given magnitude is occurring). Second, we evaluated the probability of tephra accumulation at given coordinates, based on the probability of occurrence of an eruption of a given magnitude in a given time window (nodes 1–3), in an attempt to produce useful information for long-term land-use planning.

4.1 Eruption probability

Assessing the long-term probability of an eruption is usually based on the assumption of a constant eruptive rate over a time period considered (Jones et al. 1999; Dzierma and Wehrmann 2010; Swindles et al. 2011). As a result, we used the GVP database to infer the eruptive behaviour at Cotopaxi. In this particular case, and as described above, we chose to consider eruptions of VEI 3 to 5, corresponding to bulk tephra volumes of 0.01−10 km^3 (Newhall and Self 1982).

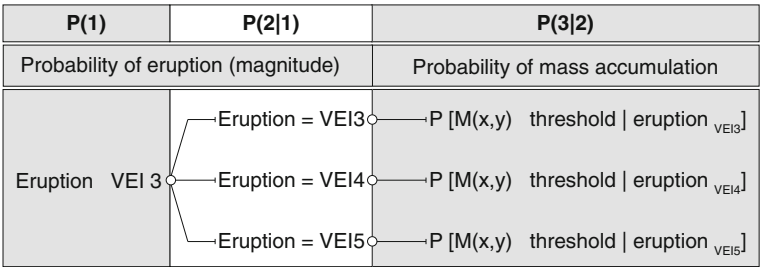

Fig. 5 Event tree used in this study considering that an eruption of a given intensity is occurring (node 3), and considering a long-term probability where the return period of eruptions of VEIs 3, 4 and 5 is evaluated in a given time window

During the Holocene, magmatism at Cotopaxi has periodically switched from rhyolitic to andesitic, with andesitic magmatism dominating the last 4,000 years (Hall and Mothes 2008). In order to guarantee the conditions of a constant eruptive rate, it is necessary to discard all data points that occurred before this change in eruptive style, fixing the beginning of the relevant catalogue at 4,000 years B.P. Figure 2a shows the cumulative eruptive history of Cotopaxi for this time period for all VEI classes considered here. As described by Simkin and Siebert (1994), this type of data shows easily definable breakpoints in the eruptive rate corresponding to different degrees of completeness of the eruptive record (vertical dashed lines in Fig. 2). As a result, the flattest trend is characterized by lack of observations where only the largest eruptions are recorded, whereas the steepest slope corresponds to a more complete record including historical reports and the preservation of smaller eruptive events. Breakpoints for VEIs 3 and 4 were defined at 1698 AD and 1350 AD, respectively, whereas VEI 5 occurred only once during this time period. The ratio of number of events over the time period considered represents the yearly eruption rate (λ), which are 3.5×10^{-2}, 9.0×10^{-3} and 2.5×10^{-4} eruption per year for VEI 3, 4 and 5, respectively. In order to aggregate the three magnitude subsets, we interpolated the different record length to the longest time period (namely 4,000 years), assuming a constant eruption rate. The resulting yearly eruption rate for VEI $\geq$3 is 4.5×10^{-2} eruption per year, yielding an average recurrence interval of 22 years (Jenkins et al. 2012a, b).

Different models have been proposed to describe random patterns of activity at explosive volcanoes (De la Cruz-Reyna 1993; Jones et al. 1999; Mendoza-Rosas and la Cruz-Reyna 2008; Dzierma and Wehrmann 2010). For simplicity, we chose to calculate long-term probabilities assuming that volcanic eruptions are stochastic processes that can be described by a Poisson distribution. Such a distribution requires that events must be independent and may occur only one at a time, and the probability of an event occurring in the next small time increment does not depend on the time that has already elapsed since the last event occurred (Borradaile 2003; Dzierma and Wehrmann 2010; Swindles et al. 2011). In the context of forecasting volcanic eruptions, we are interested in the probability that an observed repose time T is smaller than or equal to an hypothetical time period t (Dzierma and Wehrmann 2010; Swindles et al. 2011):

$$F(t) = P(T \geq t) \tag{1}$$

The simplest case of a Poisson process results in an exponential distribution:

Table 2 Probabilities of occurrence of eruptions of given VEI classes for the next 10 and 100 years (P_{10y} and P_{100y}, respectively)

	Completeness (year)	Nb. events	% tot.	λ (erup./year)	P_{10y}	P_{100y}
VEI $\geq$3	4,000	178[a]	0.045	100	0.362	0.989
VEI = 3	312	11	0.035	79	0.286	0.781
VEI = 4	660	6	0.009	20.4	0.074	0.202
VEI = 5	4,000	1	0.00025	0.6	0.002	0.006

The probability of occurrence of each VEI class is calculated as the ratio of number of eruptions of each single VEI with respect to the total number of eruptions of VEI $\geq$3. The completeness represents the period in which the eruptive activity is representative of the entire period of interest at a given volcano and was defined from Fig. 2. The number of events corresponds to the number of eruptions within the complete period. λ is the eruption rate and is assumed to be constant over the period of interest. The total percentage is the relative proportion of occurrence of each VEI class (interpolated to the longest period of completeness, i.e. 4,000 years) over the number of VEI $\geq$3

[a] Result of the sum of the interpolations of each VEI to the longest period of completeness, that is, 4,000 years

$$F_{\exp}(t) = 1 - e^{-\lambda t} \tag{2}$$

where t is the forecasting time window and λ is the yearly eruption rate.

In order to satisfy the conditions of a Poisson process, we investigated the independence of our time series with auto-correlation functions, concluding that there was not enough statistical evidence to discard the null hypothesis that events are uncorrelated (using a Student t test at the 5 % level of confidence). Second, to avoid the occurrence of two or more events at the same time, we used equation 2 to calculate the probability of occurrence of an eruption of VEI $\geq$3 for the next 10 and 100 years (Table 2), which are 0.362 and 0.989, respectively. The probability of occurrence of each separate VEI was then calculated as the relative proportion of events of each VEI class to the entire interpolated eruption catalogue (Table 2).

4.2 Modelling framework

Following Bonadonna (2006), we adopted here a probabilistic approach using the advection-diffusion model TEPHRA2 (Bonadonna et al. 2005). The model was used on a cluster of computers, comprising a total of 32 CPUs and manually parallelized. Resulting probability maps contour the probability of reaching a given hazardous threshold of tephra accumulation for a defined eruptive scenario. The compilation of such maps consists in running the model a sufficient amount of times, stochastically sampling at each run a wind profile within a relevant population of wind profiles, and/or a set of physical parameters (i.e. plume height, erupted mass, median grainsize) within a predefined range, through the use of Monte-Carlo techniques (e.g. Hurst and Smith 2004). Best values of the number of runs and size of the wind population can be inferred from plots similar to Fig. 6 and will be discussed below.

The analytical model TEPHRA2 requires several empirical input parameters that cannot be derived from field observations, namely the diffusion coefficient and the fall-time threshold for change in diffusive behaviour. These parameters were inferred using analytical inversion techniques (Biass and Bonadonna 2011).

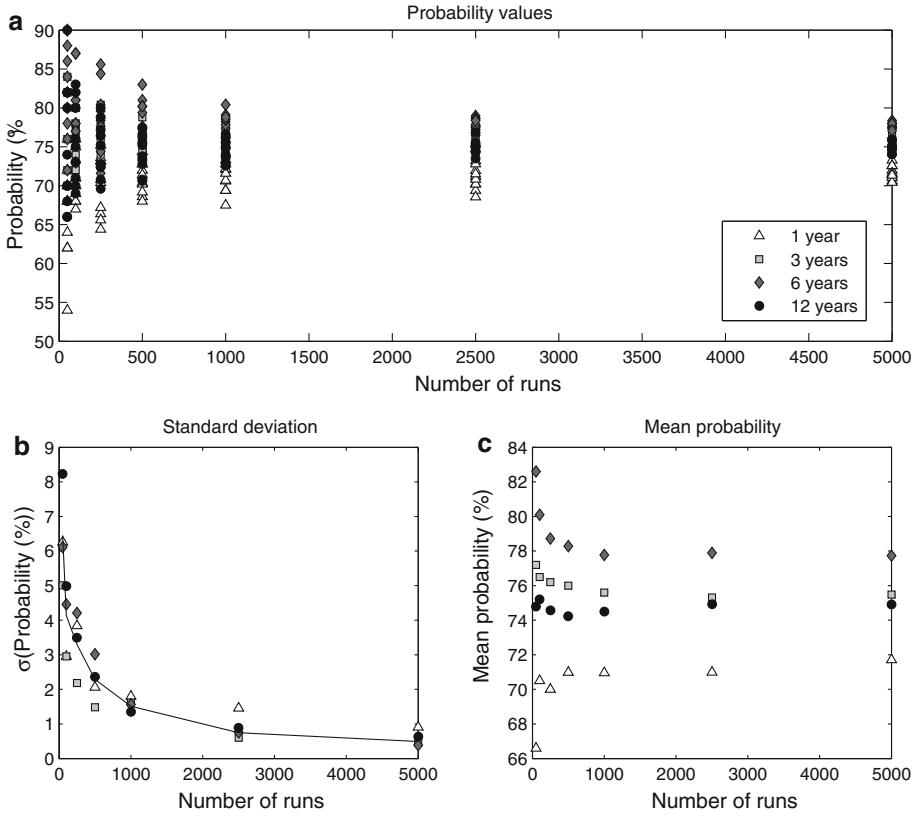

Fig. 6 Accuracy of the Monte-Carlo techniques used to compile ERS assessments following the strategy of Bonadonna et al. (2002). Variability of **a** the probability of exceeding an accumulation of 10 kg/m^2; **b** standard deviation and **c** mean probability values

4.2.1 Eruption scenarios

Two types of eruption scenarios were considered in this study, both contouring the probability of reaching a given tephra accumulation around the volcano:

$$P[M(x, y) \geq \text{threshold} | \text{eruption}] \tag{3}$$

where $M(x, y)$ is the mass of tephra accumulation (kg/m^2) at a given location (x, y).

One Eruption Scenario (OES) The OES is a semi-probabilistic approach that compiles the probability of reaching a given hazardous threshold of tephra accumulation with a varying wind, where eruptive parameters are deterministically defined. This method is useful to evaluate the possible impacts of a known studied eruption. We used two reference eruptions of Cotopaxi for the OES runs: Layer 3 and Layer 5, defined by Barberi et al. (1995) and fully characterized by Biass and Bonadonna (2011). Physical eruptive parameters are summarized in Table 3.

Eruption Range Scenario (ERS) The ERS describes the probability of reaching a given tephra accumulation based on the statistical distribution of both wind profiles and eruptive parameters. Based on the VEI frequency distribution of Cotopaxi volcano (Fig. 2a), we

Table 3 Source term parameters for each eruptive scenario used in the modelling

	Ht (km a.s.l.)	Mass (kg)	Mdϕ	$\sigma\phi$
OES Layer 3	29	1.7×10^{12}	−0.5	1.7
OES Layer 5	29	4.5×10^{11}	0.6	2.5
ERS VEI 3	10–20	$1-10 \times 10^{10}$	−1 to 3	2.5
ERS VEI 4	15–30	$1-10 \times 10^{11}$	−1 to 3	2.5
ERS VEI 5	25–35	$1-10 \times 10^{12}$	−1 to 3	2.5

Values of plume height and erupted mass used for ERS modelling are based on the VEI scale of Newhall and Self (1982). ϕ is a measure of the grainsize, which is $\log_2$(diameter [mm]). Mdϕ and $\sigma\phi$ are the median and the standard deviation of the grainsize respectively (Inman 1952). Minimum and maximum grainsize values deterministically fixed (8ϕ and −4ϕ, respectively)

decided to focus on VEI 3, 4 and 5. The VEI scale (Newhall and Self 1982) is mainly constrained by values of erupted tephra but is also related to specific ranges of plume height. We used these boundary values of plume height and erupted tephra to run ERS for each VEI (see Table 3).

4.2.2 Accuracy of Monte-Carlo techniques

Probabilistic hazard assessments are computationally expensive and are ideally performed using parallel processing on a cluster of computers. It is necessary to assess the variability of Monte-Carlo techniques with varying number of runs and wind profiles, in order to find the best compromise between the number of runs to consider and accuracy of the output. Figure 6a shows the probability calculation of reaching 10 kg/m^2 at a given point located 20 km downwind from the vent, with different number of wind profiles and number of runs. The total wind population (1997–2008) was divided in smaller subsets of 1, 3, 6 and 12 years. For each wind subset, 10 series of simulations were performed, varying the number of runs between 10 to 5,000. In order to avoid the duplicate patterns of random numbers, every set of run was performed based on a different probability seed. Figure 6b shows the decreasing trend of the standard deviation with the number of runs, with the smallest discrepancy amongst wind subsets around 1,000 runs. Figure 6c shows the variability of the mean probability value amongst wind subsets with the number of runs performed. From Fig. 6c, we could conclude that (i) a stability of values of mean probability can be observed above 1,000 runs and (ii) the mean probability using a wind population of 12 years is the most constant throughout the number of runs. As a result, we have chosen to perform 1,000 runs with the whole population of wind (12 years) for each eruptive scenario in order to obtain the best compromise between computation time and output accuracy.

5 Results

The resulting hazard assessment was compiled using three complementary techniques: probability maps based on hazardous accumulation thresholds, isomass maps based on critical probability thresholds and hazard curves.

Probability maps based on an eruption scenario contour the probability of reaching a given tephra accumulation. Critical values of tephra accumulation can be based on the

effects of fallout observed for a number of eruptive events and volcanoes. In this study, two values of 10 and 100 kg/m^2 were used, which are critical for light damage to crops and the onset of structural damages of the weakest roofs, respectively (Blong 1984; Wilson et al. 2011a). As an example, OES for Layer 5 and ERS of VEI 4 have been used as an illustration for two medium intensity explosive eruptions (Fig. 7a, b). These maps show how Quito has a <10 % probability to reach an accumulation of 10 kg/m^2 of tephra for the ERS of VEI 4, whereas Latacunga has a probability of about 50 % for the same tephra threshold and scenario (Fig. 7b). The multi-VEI ERS probability maps are compiled by summing the products of the probability matrix of ERS for each separate VEI class with their respective probability of occurrence (Table 2). Figure 7c illustrates this concept using ERS of VEI 3, 4 and 5 in a time window of 100 years (Table 2) and shows that Quito and Latacunga have probabilities of reaching a total accumulation of tephra of 10 kg/m^2 in the next 100 years of about <10 and 30 %, respectively.

Probability maps for a given tephra threshold are reshaped into isomass maps of a given probability (Fig. 7d), which is important when producing risk maps (Biass et al., this volume). The choice of a significant probability threshold is, however, complex and could be regarded as the *acceptable losses* that authorities would consider for a given exposed population. As an example, we chose an arbitrary probability threshold of 50 % to illustrate the use of this technique. Figure 7d shows the resulting isomass map for the ERS of

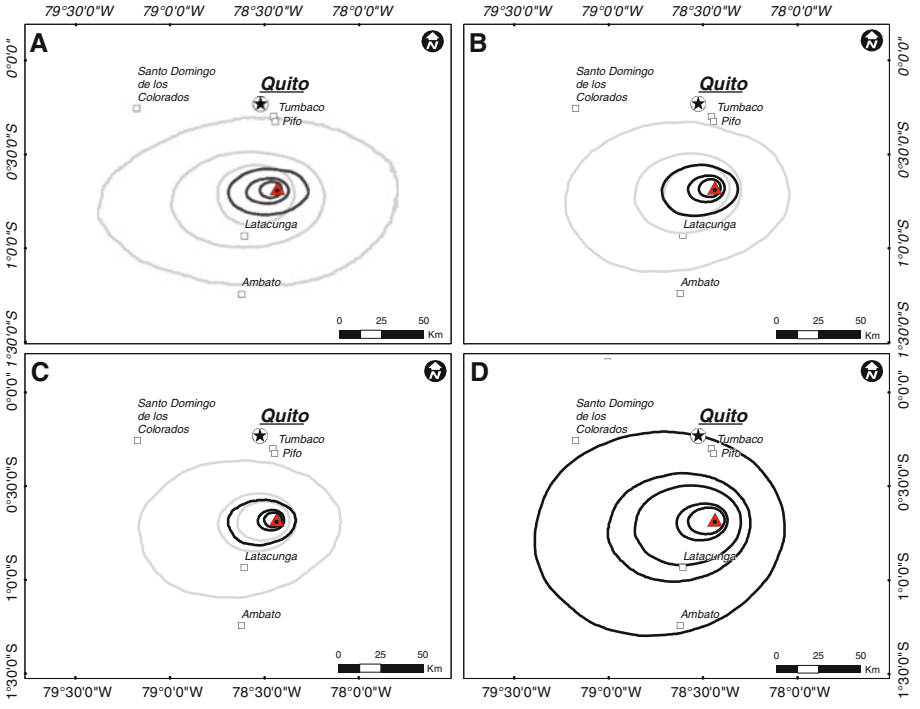

Fig. 7 Hazard maps showing the probability of reaching a given mass accumulation (**a–c**) and isomass map for a given probability threshold (**d**). **a–c** Probability contours (10, 50 and 80 %) for thresholds of 10 kg/m^2 (*light grey*) and 100 kg/m^2 (*dark grey*) for **a** OES for Layer 5, **b** ERS of VEI 4 and **c** multi-VEI ERS for a time window of 100 years. **d** Isomass contours (1, 5, 10, 50 and 100 kg/m^2) for an ERS of VEI 4 and a probability threshold of 50 %

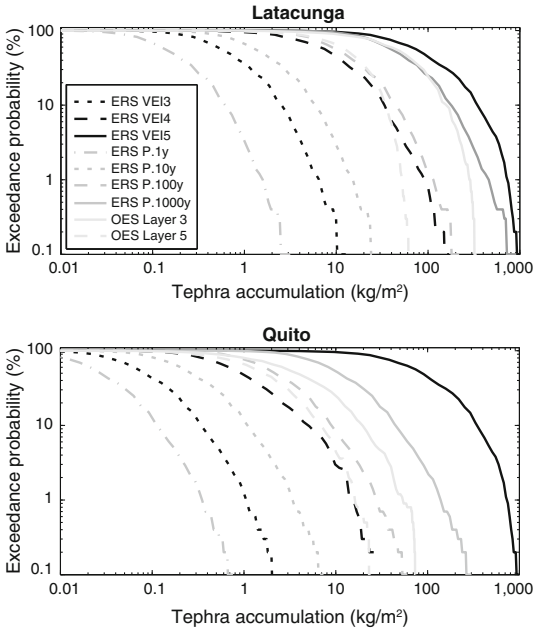

Fig. 8 Hazard curves for the cities of Latacunga and Quito (see Fig. 1), showing the exceeding probability for all different eruptive scenarios modelled in the hazard assessment. Eruptive scenarios are ERS for individual VEI classes (*black lines*), multi-VEI ERS (*medium grey lines*) and OES (*light grey lines*)

VEI 4 for a probability threshold of 50 %, where Quito and Latacunga display accumulations of 1 and 10 kg/m^2, respectively. To illustrate the variability of the resulting maps due to the choice of the probability threshold, isomass maps for an ERS of VEI 4 with probability thresholds of 30 and 70 % can be found in Online Resource 1.

All scenarios were also used to produce hazard curves, which describe the probability of exceeding certain values of tephra accumulation for a given location (Bonadonna 2006). Figure 8 shows hazard curves for the cities of Quito and Latacunga.

Table 4 shows the area covered by the different isomass lines for all scenarios considered in this hazard assessment. It also shows the destructiveness index, defined by Pyle (2000) as the $\log_{10}$ of the area covered by the 100 kg/m^2 isomass, value usually related to roof collapse. Table 5 shows the number of people affected by the same mass loading, as inferred from the Landscan 2005 dataset.

6 Discussion

The combined use of numerical modelling, probabilistic strategies and detailed field observations allowed the development of a comprehensive set of possible eruption scenarios at Cotopaxi volcano. These were used as a first step to evaluate the impact of future volcanic activity in the area. The distribution of wind profiles explains why high values of probabilities and tephra accumulation are concentrated westwards (see Figs. 3, 4, 7). As a result, the region located west of Cotopaxi volcano and between Quito and Latacunga will likely be exposed to moderate to heavy tephra accumulation in the case of an eruption, resulting in possible health issues, blockage of air traffic and roads, damage to crops and agriculture and structural damage to buildings and roofs. A detailed study of the impact of tephra fallout in this region can be found in Biass et al. (this volume).

Table 4 Area covered by 1, 10, 100 and 300 kg/m^2 for each scenario compiled, assuming a 50 % probability

	Area for isomass (km^2)				Destructiveness index
	1 kg/m^2	10 kg/m^2	100 kg/m^2	300 kg/m^2	
OES 3	42,234	10,749	1,587	565	3.2
OES 5	28,935	3,957	284	74	2.5
ERS VEI 3	2,094	298	27	–	1.4
ERS VEI 4	13,874	2,305	264	91	2.4
ERS VEI 5	80,639	17,940	2,364	691	3.4
ERS 100 y	7,922	1,225	147	47	2.2

The destructiveness index of Pyle (2000), calculated as the $\log_{10}$ of the area covered by the 100 kg/m^2 isomass, is also shown. ERS 100 y stands for the ERS scenarios compiled with a probability of occurrence in the next 100 years

Table 5 Number of people potentially affected by the different mass loading, inferred from the Landscan 2005 dataset, for a probability threshold of 50 %

	People affected by tephra loading			
	1 kg/m^2	10 kg/m^2	100 kg/m^2	300 kg/m^2
OES 3	548,993	68,966	11,646	2,685
OES 5	437,607	38,747	5,724	183
ERS VEI 3	17,695	5,583	19	–
ERS VEI 4	230,942	21,290	4,415	313
ERS VEI 5	824,148	269,746	18,596	2,689
ERS 100 y	69,587	6,001	1,495	95

6.1 Hazard assessment

The past two decades have been characterized by significant improvements in strategies of volcanic hazard assessment, which are typically made complicated by the fact that volcanoes are multi-hazard systems. The assessment of the degree of variability of each hazardous phenomenon is required to define relevant eruption scenario, on the basis of which phenomenon will be tackled with deterministic or stochastic approaches (Bonadonna 2006). As a result, most recent hazard assessments tend to include a combination of field studies, numerical modelling and geo-informatic tools (i.e. GIS platforms). Although they are the starting point of any study, field campaigns are often costly and logistically difficult, especially in remote areas. Single field seasons usually focus on the study of a single eruption, or a few eruptions at most. In this context, the GVP continues to compile most published data into a single database of known eruptions. As a result, the combined use of global databases such as the GVP as a catalogue of known eruptions and the NOAA Reanalysis 1 for wind profiles along with the VEI-based ERS method presented here allows for a fast and comprehensive assessment of the hazard related to tephra fallout, even when a limited number or no field data is available. The GVP database makes it possible to evaluate the probability of the occurrence of an eruption of a given size, that can be incorporated in probability trees to assess the long-term effect of tephra fallout (Fig. 5). Additionally, we also show how the availability of accurate field investigations can be used in order to calibrate the ERS strategy and to provide

hazard scenarios based on reference eruptions (OES). Limitations are inherent to the use of such global databases, as they provide "some of our best clues in interpreting Earth's volcanism" (Siebert et al. 2010, p. 31), and should be viewed as complementary to detailed field investigations. Similarly, due to the difficulty of accessing direct measurements of wind profiles, the NOAA Reanalysis 1 database is a convenient database to statistically infer global wind patterns over a long period of time. Wind patterns resulting from this database provide large-scale dispersal trends but fail to describe small-scale wind variations around a volcano, which can often be important factors in the distribution of ash and lapili.

Given the general difficulty to effectively communicate hazard levels (Newhall 2000; Haynes et al. 2007), we used three different outputs to describe our hazard assessment. First, we produced probability maps, which contour the probability of exceeding a given tephra accumulation for a given eruptive scenario (Fig. 7a–c). This tool helps to identify the spatial variability of the likelihood of reaching a tephra accumulation of interest for a given scenario. For example, the dark grey lines of Fig. 7b are the 10, 50 and 80 % probability of reaching an accumulation of 100 kg/m^2 for an ERS of VEI 4 and show that buildings located about 10 km west of Cotopaxi have a 70 % probability of suffering structural damage (up to possible roof collapse), in contrast to a 10 % probability for buildings located 25 km in the same direction. Second, we produced isomass maps for a given probability threshold, which are helpful for producing rapid exposure-based assessments of potential damage associated with an eruption (Fig. 7d). Such maps require the delicate choice of a probability threshold, which is in practice defined by decision-makers on the basis of cost-benefit analysis (Marzocchi and Woo 2009). The choice of acceptable losses goes beyond the scope of this paper, and a theoretical probability threshold of 50 % is considered in this study. Finally, the hazard assessment is displayed using hazard curves, which are used to evaluate the hazard at a given location. Hazard curves are more flexible than probability maps, as they do not rely on the choice of hazardous thresholds of tephra accumulation. Figure 8 shows hazard curves for all eruptive scenarios for two important urbanized centres, namely Quito and Latacunga. At local scales, this tool is useful to identify exposed elements independently from fixed thresholds, which is necessary for both mitigation measures and the development of evacuation routes.

6.2 Importance of probabilistic strategies

Field investigations are a crucial step towards constraining the eruptive style of a volcano, but they have several limitations. For example, the eruptive history of a given volcano inferred from the geological record is biased towards large events, as small eruptions will produce minimal tephra deposits that will be quickly removed by erosion (Fig. 2). Also, field observations can only provide a sub-sample of the possible range of eruptive parameters such as plume height, erupted mass and weather conditions. The existing hazard maps for tephra fallout for Cotopaxi volcano contour the tephra thickness expected for an eruption of moderate size, using deterministically chosen eruptive parameters and a typical wind profile (Hall and Hillebrandt 1988). Hazard assessments based on field observations result in an incomplete picture failing to describe the whole range of possible impacts of future activity. In contrast to such deterministic methods, probabilistic approaches based on Monte-Carlo simulations can help to extrapolate the sub-samples of eruptive parameters and weather conditions inferred from field observation into statistically representative populations suitable for hazard assessments. The combined use of weather databases such as the NCEP/NCAR Reanalysis 1 (Kalnay et al. 1996) and stochastic sampling provides a realistic picture of the weather conditions for a given area, based

on decades of observations. The stochastic sampling of eruptive parameters also helps to assess a wide range of possible outcomes of an eruption. Any probability density function can be used to sample eruptive parameters and can be either defined deterministically, when sufficient field data are available, or using Monte-Carlo simulations based on the few data available (Hurst and Smith 2004). Probabilistic methods and random processes should not be used without a solid calibration based on observations. Figure 6 provides an indication of the critical number of wind profiles required to significantly capture the intrinsic variability of wind patterns, as well as insights into the number of model runs needed to provide stable results. From this method, a population of 12 years of wind was proved to provide the most stable probability values with varying numbers of runs (maximum variability of mean probability values of 1.5 %, Fig. 6). Similarly, model 1,000 runs provide a good compromise between stability of results and computation time (e.g. variability of the standard deviation within 0.5 %; Fig. 6b), which is consistent with values obtained on Soufriere Hills, Montserrat (Bonadonna et al. 2002). Here, sampling of eruptive parameters was based on the values of tephra mass and plume height defined by the VEI scale. Plume heights and erupted masses were stochastically sampled based on a logarithmic distribution in order to give more importance to small events, whereas grainsize parameters were stochastically sampled on a linear scale. As a result, we present two extremes in the assessment of the hazard related to tephra fallout. On one hand, traditional hazard assessments typically use numerical models, for which input parameters are deterministically defined based on detailed field investigations. On the other hand, the use of ERS strategies based on VEI classes combined with global databases allows for a rapid and remote evaluation of the hazard related with tephra fallout. However, the VEI scale cannot be considered as universal as it relies on a simple and often unrealistic assumption of a constant relationship between the erupted mass and the plume height (Pyle 2000). As a result, boundary values of mass and plume height defined by the VEI scale are not absolute, and field data can be used in ERS methods to adjust the sampling range of eruptive parameters.

6.3 Eruptive scenarios

Figure 5 serves as a framework for conditional probabilities used in this hazard assessment. As previously discussed, probabilities at nodes 1 and 2 can be assessed using the GVP database. Node 3 evaluates the expected range of tephra accumulation over a region of interest, assuming the occurrence of a specific eruption scenario (i.e. probability = 1 at node 2 for a given magnitude of eruption). Figure 5 in its complete form is useful for VEI-based ERS strategies. In contrast, OES approaches focus on node 3 as they are based on studied eruptions, for which it is not possible to assign a probability of occurrence. The available field investigations for Cotopaxi volcano allowed for probabilistic modelling of two known eruptions of VEI 4 and 5 (OES, Table 3), whereas three ERS have been defined using the VEI scale. Table 5 illustrates the difference between scenarios where the eruptive parameters are set deterministically (Layer 3: low VEI 5; Layer 5: high VEI 4) and using probability density functions. As an example, the number of people affected by any tephra accumulation for a Layer 3 OES is lower than considering an ERS of VEI 5. In fact, Layer 3 is a single case of an eruption of VEI 5 of moderate intensity. Similarly, the number of affected people is always higher when the Layer 5 OES is compared to an ERS of VEI 4, because Layer 5 is a single occurrence of a strong eruption of VEI 4 at the boundary with VEI 5. As a result, eruption scenarios defined in Table 3 aim to provide a complete picture of possible future eruptive patterns, based on both deterministic (i.e. accurate field data) and stochastic (i.e. Monte-Carlo simulations) strategies.

7 Conclusions

This study provides a comprehensive hazard assessment of Cotopaxi volcano, in combination with a new strategy based on global data for the hazard assessment of volcanoes with only little available information. Two complementary approaches have been used to produce a comprehensive hazard assessment. First, five eruption scenarios have been considered: (i) two scenarios based on detailed field data where input eruptive parameters were deterministically defined (OES for Layer 3 and OES for Layer 5) and (ii) three scenarios based on ranges of values for erupted volume and plume height defined by the VEI scale, where VEI 3, 4 and 5 have been recognized as being the most frequent hazardous events at Cotopaxi volcano (GVP; Siebert and Simkin 2002). The stochastic sampling of 1,000 wind profiles out of 12 years of wind for each scenario was shown to provide a good compromise between output stability and computation time (within 0.8 % discrepancy, Fig. 6). Second, the occurrence probability of each VEI class was assessed based on the GVP database and used to combine the ERS of each VEI class to produce a long-term assessment of the probability of tephra accumulation at different time windows.

A new way of displaying the resulting hazard assessment is proposed, which consists in producing isomass maps for a given probability. This method helps to highlight the most dangerous areas around the vent and facilitates the integration in further risk analysis (Biass et al. this volume). In the case of Cotopaxi volcano, even eruptions of moderate size (VEI 3) can potentially affect thousands of people. The two eruptions used as benchmark in this study would have today a 50 % probability of affecting $\sim$550,000 and $\sim$440,000 people (Layer 3 and Layer 5 respectively).

Acknowledgments This research was possible thanks to the generous support of the Fondation Marc Birkigt, Geneva (S. Biass). We are grateful to William Aeberhard and Corine Frishcknecht for the invaluable scientific discussions and to two anonymous reviewers whose comments greatly improved this manuscript.

References

Aguilera E, Pareschi MT, Rosi M, Zanchetta G (2004) Risk from lahars in the northern valleys of Cotopaxi Volcano (Ecuador). Nat Hazards 33(2):161–189

Barberi F, Caruso P, Macedonio G, Pareschi M, Rosi M (1992) Reconstruction and numerical simulation of the lahar of the 1877 eruption of Cotopaxi volcano (Ecuador). Acta Vulcanol 2:35–44

Barberi F, Coltelli M, Frullani A, Rosi M, Almeida E (1995) Chronology and dispersal characteristics of recently (last 5000 years) erupted tephra of Cotopaxi (Ecuador): implications for long-term eruptive forecasting. J Volcanol Geotherm Res 69(3–4):217–239

Biass S, Bonadonna C (2011) A quantitative uncertainty assessment of eruptive parameters derived from tephra deposits: the example of two large eruptions of Cotopaxi volcano, Ecuador. Bull Volcanol 73(1):73–90

Blong R (2003) Building damage in Rabaul, Papua New Guinea, 1994. Bull Volcanol 65(1):43–54

Blong RJ (1984) Volcanic hazards. A sourcebook on the effects of eruptions. Academic Press, Orlando

Bonadonna C (2006) Probabilistic modelling of tephra dispersion. In: Mader HM, Coles SG, Connor CB, Connor LJ (eds) Statistics in volcanology, Special Publications of IAVCEI, vol 1. Geological Society of London, London, pp 243–259

Bonadonna C, Macedonio G, Sparks RSJ (2002) Numerical modelling of tephra fallout associated with dome collapses and Vulcanian explosions: application to hazard assessment on Montserrat. In: Druit T, Kokelaar B (eds) The eruption of Soufriere Hills Volcano, Montserrat, from 1995 to 1999, The Geological Society, London, Memoirs, vol 21. The Geological Society of London, London, pp 517–537

Bonadonna C, Connor CB, Houghton BF, Connor L, Byrne M, Laing A, Hincks TK (2005) Probabilistic modeling of tephra dispersal: hazard assessment of a multiphase rhyolitic eruption at Tarawera, New Zealand. J Geophys Res 110(10.1029):B03203

Borradaile GJ (2003) Statistics of earth science data: their distribution in time, space, and orientation. Springer, Berlin

Chester DK, Degg M, Duncan AM, Guest JE (2000) The increasing exposure of cities to the effects of volcanic eruptions: a global survey. Environ Hazard 2(3):89–103

Connor CB, Hill BE, Winfrey B, Franklin NM, La Femina PC (2001) Estimation of volcanic hazards from tephra fallout. Nat Hazard Rev 2(1):33–42

De la Cruz-Reyna S (1993) Random patterns of occurrence of explosive eruptions at Colima Volcano, Mexico. J Volcanol Geotherm Res 55(1–2):51–68

D'Ercole R (1996) Représentations cartographiques des facteurs de vulnérabilité des populations exposées à une menace volcanique. Application à la région du volcan Cotopaxi (Equateur). Bull Inst fr études andines 25(3):479–507

D'Ercole R, Demoraes F (2003) Risques et réponses institutionnelles en Equateur–Cartes et méthodes. Cahiers de Géographie Collect EDYTEM 1:157–168

Dzierma Y, Wehrmann H (2010) Eruption time series statistically examined: probabilities of future eruptions at Villarrica and Llaima Volcanoes, Southern Volcanic Zone, Chile. J Volcanol Geotherm Res 193(1–2):82–92

EM-DAT (2011) EM-DAT: The OFDA/CRED International Disaster Database. http://www.emdat.be. Accessed 12 Feb 2011

Fournier d'Albe EM (1979) Objectives of volcanic monitoring and prediction. J Geol Soc Lond 136:321–326

Guffanti M, Mayberry GC, Casadevall TJ, Wunderman R (2009) Volcanic hazards to airports. Nat Hazards 51(2):287–302

Hall M, Hillebrandt vC (1988) Mapa de los peligros volcanicos potenciales asociados con el volcan cotopaxi: (1) zona norte and (2) zona sur. Instituto Geofisico, Quito

Hall M, Mothes P (2008) The rhyolitic–andesitic eruptive history of Cotopaxi volcano, Ecuador. Bull Volcanol 70(6):675–702

Haynes K, Barclay J, Pidgeon N (2007) Volcanic hazard communication using maps: an evaluation of their effectiveness. Bull Volcanol 70(2):123–138. doi:10.1007/s00445-007-0124-7

Hellström T (2007) Critical infrastructure and systemic vulnerability: towards a planning framework. Saf Sci 45(3):415–430

Hill BE, Connor CB, Jarzemba MS, La Femina PC, Navarro M, Strauch W (1998) 1995 eruptions of Cerro Negro volcano, Nicaragua, and risk assessment for future eruptions. Geol Soc Am Bull 110(10):1231

Horwell CJ, Baxter PJ (2006) The respiratory health hazards of volcanic ash: a review for volcanic risk mitigation. Bull Volcanol 69(1):1–24

Horwell CJ, Sparks RSJ, Brewer TS, Llewellin EW, Williamson BJ (2003) Characterization of respirable volcanic ash from the Soufrière Hills volcano, Montserrat, with implications for human health hazards. Bull Volcanol 65(5):346–362

Hurst T, Smith W (2004) A Monte Carlo methodology for modelling ashfall hazards. J Volcanol Geotherm Res 138(3–4):393–403

Inbar M, Ostera HA, Parica CA, Remesal MB, Salani FM (1995) Environmental assessment of 1991 Hudson volcano eruption ashfall effects on southern Patagonia region, Argentina. Environ Geol 25(2):119–125

Inman DL (1952) Measures for describing the size distribution of sediments. J Sediment Res 22(3):125–145

Jenkins S, Magill C, McAneney J, Blong R (2012a) Regional ash fall hazard I: a probabilistic assessment methodology. Bull Volcanol 1–14. doi:10.1007/s00445-012-0627-8

Jenkins S, McAneney J, Magill C, Blong R (2012b) Regional ash fall hazard II: Asia-pacic modelling results and implications. Bull Volcanol 1–15. doi:10.1007/s00445-012-0628-7

Johnston DM, Houghton BF, Neall VE, Ronan KR, Paton D (2000) Impacts of the 1945 and 1995–1996 Ruapehu eruptions, New Zealand: an example of increasing societal vulnerability. Geol Soc Am Bull 112(5):720–726

Jones G, Chester DK, Shooshtarian F (1999) Statistical analysis of the frequency of eruptions at Furnas Volcano, São Miguel, Azores. J Volcanol Geotherm Res 92(1–2):31–38

Kalnay EC, Kanamitsu M, Kistler R, Collins W, Deaven D, Gandin L, Iredell M, Saha S, White G, Woollen J (1996) The NCEP/NCAR 40-year reanalysis project. Bull Am Meteorol Soc 77(3):437–471

Marti J, Spence R, Calogero E, Ordo ez A, Felpeto A, Baxter P (2008) Estimating building exposure and impact to volcanic hazards in Icod de los Vinos, Tenerife (Canary Islands). J Volcanol Geotherm Res 178(3):553–561

Martin RS, Watt SFL, Pyle DM, Mather TA, Matthews NE, Georg RB, Day JA, Fairhead T, Witt MLI, Quayle BM (2009) Environmental effects of ashfall in Argentina from the 2008 Chaitén volcanic eruption. J Volcanol Geotherm Res 184(3–4):462–472

Marzocchi W, Woo G (2009) Principles of volcanic risk metrics: theory and the case study of Mount Vesuvius and Campi Flegrei, Italy. J Geophys Res 114(B3):B03,213

Mendoza-Rosas AT, la Cruz-Reyna S (2008) A statistical method linking geological and historical eruption time series for volcanic hazard estimations: applications to active polygenetic volcanoes. J Volcanol Geotherm Res 176(2):277–290

Millard GA, Mather TA, Pyle DM, Rose WI, Thornton B (2006) Halogen emissions from a small volcanic eruption: modeling the peak concentrations, dispersion, and volcanically induced ozone loss in the stratosphere. Geophys Res Lett 33:33–34

Moteff J, Copeland C, Fischer J (2003) Critical infrastructures: what makes an infrastructure critical? Report for Congress RL31556, Congressional Research Service, Library of Congress, Washington, DC, Accessed 13 Feb 2011

Mothes P, Hall ML, Andrade D, Samaniego P, Pierson TC, Ruiz AG, Yepes H (2004) Character, stratigraphy and magnitude of historical lahars of Cotopaxi Volcano (Ecuador). Acta Vulcanol 16(1/2):85

Neri A, Aspinall WP, Cioni R, Bertagnini A, Baxter PJ, Zuccaro G, Andronico D, Barsotti S, Cole PD, Esposti Ongaro T (2008) Developing an event tree for probabilistic hazard and risk assessment at Vesuvius. J Volcanol Geotherm Res 178(3):397–415

Newhall C (2000) Volcano warnings. In: Sigurdsson H, Houghton BF, Ballard RD (eds) Encyclopedia of volcanoes. Academic Press, London, pp 263–269

Newhall C, Hoblitt R (2002) Constructing event trees for volcanic crises. Bull Volcanol 64(1):3–20

Newhall CG, Self S (1982) The volcanic explosivity index/VEI/—an estimate of explosive magnitude for historical volcanism. J Geophys Res 87(C2):1231–1238

Pistolesi M, Rosi M, Cioni R, Cashman KV, Rossotti A, Aguilera E (2011) Physical volcanology of the post-twelfth-century activity at Cotopaxi volcano, Ecuador: behavior of an andesitic central volcano. Geol Soc Am Bull 123(5-6):1193–1215. doi:10.1130/B30301.1

Pomonis A, Spence R, Baxter P (1999) Risk assessment of residential buildings for an eruption of Furnas Volcano, Sao Miguel, the Azores. J Volcanol Geotherm Res 92(1–2):107–131

Pyle DM (2000) Sizes of volcanic eruptions. In: Sigurdsson H, Houghton BF, Ballard RD (eds) Encyclopedia of volcanoes. Academic Press, London, pp 263–269

Robock A (2000) Volcanic eruptions and climate. Rev Geophys 38(2):191–219

Siebert L, Simkin T (2002) Volcanoes of the world: an illustrated catalog of holocene volcanoes and their eruptions. Smithsonian Institution, Global Volcanism Program Digital Information Series, GVP-3 URL http://www.volcano.si.edu/world

Siebert L, Simkin T, Kimberly P (2010) Volcanoes of the World. University of California Press, London

Simkin T, Siebert L (1994) Volcanoes of the World. Geoscience Press, Tucson

Small C, Naumann T (2001) The global distribution of human population and recent volcanism. Environ Hazard 3(3–4):93–109. doi:10.1016/S1464-2867(02)00002-5. URL: http://www.sciencedirect.com/science/article/pii/S1464286702000025

Spence RJS, Pomonis A, Baxter PJ, AW C (1996) Building damage caused by the Mount Pinatubo eruption of June 15, 1991. University of Washington Press, Seattle, pp 1053–1061

Spence RJS, Kelman I, Baxter PJ, Zuccaro G, Petrazzuoli S (2005) Residential building and occupant vulnerability to tephra fall. Nat Haz Earth Syst Sci 5(4):477–494

Swindles GT, Lawson IT, Savov IP, Connor CB, Plunkett G (2011) A 7000 yr perspective on volcanic ash clouds affecting northern Europe. Geology 39(9):887–890. doi:10.1130/G32146.110.1130/G32146.1. URL: http://geology.gsapubs.org/cgi/content/abstract/39/9/887, http://geology.gsapubs.org/cgi/reprint/39/9/887.pdf

Wilson T, Cole J, Cronin S, Stewart C, Johnston D (2011a) Impacts on agriculture following the 1991 eruption of Vulcan Hudson, Patagonia: lessons for recovery. Nat Hazards 57:185–212. doi:10.1007/s11069-010-9604-8

Wilson T, Cole J, Stewart C, Cronin S, Johnston D (2011b) Ash storms: impacts of wind-remobilised volcanic ash on rural communities and agriculture following the 1991 Hudson eruption, southern Patagonia, Chile. Bull Volcanol 73:223–239. doi:10.1007/s00445-010-0396-1

Wilson TM, Stewart C, Sword-Daniels V, Leonard GS, Johnston DM, Cole JW, Wardman J, Wilson G, Barnard ST (2012) Volcanic ash impacts on critical infrastructure. Phys Chem Earth Pt A/B/C 45–46:5–23. doi:10.1016/j.pce.2011.06.006

Zuccaro G, Cacace F, Spence RJS, Baxter PJ (2008) Impact of explosive eruption scenarios at Vesuvius. J Volcanol Geotherm Res 178(3):416–453